crystals

MDPI

Article

Performance Improvement of Amorphous Ga_2O_3/P-Si Deep Ultraviolet Photodetector by Oxygen Plasma Treatment

Jin Cao [1,†], Liang Chen [2,†], Xin Chen [1], Yu Zhu [1], Jianqi Dong [1], Baoyu Wang [1], Miao He [2,*] and Xingfu Wang [1,*]

[1] Laboratory of Nanophotonic Functional Materials and Devices, Institute of Semiconductor Science and Technology, South China Normal University, Guangzhou 510631, China; origincj@foxmail.com (J.C.); x.chen@m.scnu.edu.cn (X.C.); yuzhu@m.scnu.edu.cn (Y.Z.); j.q.dong@m.scnu.edu.cn (J.D.); by.wang@m.scnu.edu.cn (B.W.)

[2] School of Physics and Optoelectronic Engineering, Guangdong University of Technology, Guangzhou 510006, China; phliangchen@mail.scut.edu.cn

* Correspondence: lc3596@mail2.gdut.edu.cn (M.H.); xfwang@scnu.edu.cn (X.W.)

† J.C. and L.C. contributed equally to this work.

Abstract: Gallium oxide (Ga_2O_3) is an attractive semiconductor that is very suitable for deep ultraviolet (DUV) inspection. However, due to the existence of many types of oxygen vacancies in the amorphous Ga_2O_3 (a-Ga_2O_3) film, it greatly limits the performance of the a-Ga_2O_3-based photodetector. Here, we perform oxygen plasma treatment on the a-Ga_2O_3/p-Si photodetector to reduce the concentration of oxygen vacancies in the a-Ga_2O_3 film, so that the dark current is reduced by an order of magnitude (from 1.01×10^{-3} A to 1.04×10^{-4} A), and the responsivity is increased from 3.7 mA/W to 9.97 mA/W. In addition, oxygen plasma processing makes the photodetector operate well at 0 V bias. The response speed is that the rise time is 2.45 ms and the decay time is 1.83 ms, while it does not respond to the DUV illumination without oxygen plasma treating at a zero bias. These results are attributed to the fact that oxygen plasma treatment can reduce the Schottky barrier between a-Ga_2O_3 and the electrode indium tin oxide (ITO), which promotes the separation and collection efficiency of photo-generated carriers. Therefore, this work proposes a low-cost method to improve the performance of Ga_2O_3 film-based DUV photodetectors.

Keywords: oxygen vacancies; a-Ga_2O_3/p-Si heterojunction; deep ultraviolet photodetector; oxygen plasma

Citation: Cao, J.; Chen, L.; Chen, X.; Zhu, Y.; Dong, J.; Wang, B.; He, M.; Wang, X. Performance Improvement of Amorphous Ga_2O_3/P-Si Deep Ultraviolet Photodetector by Oxygen Plasma Treatment. *Crystals* **2021**, *11*, 1248. https://doi.org/10.3390/cryst11101248

Academic Editors: Haiding Sun, Bharat Jalan, Shibing Long, Yuhao Zhang, Rajendra Singh, Xuelin Yang, Yuji Zhao, Bin Liu and M. Ajmal Khan

Received: 22 August 2021
Accepted: 11 October 2021
Published: 15 October 2021

1. Introduction

Deep ultraviolet photodetectors (PDs), due to their good anti-interference property, have various applications in the fields of environmental monitoring, wireless secure communication, fire warning, and missile warning [1–5]. Deep ultraviolet PDs fabricated with wide band gap semiconductor materials such as diamond [6], AlGaN [7], AlN [8], and Ga_2O_3 have attracted increasing attention because of their excellent anti-interference performance [9–13]. However, the band gap of AlN and diamond is too wide to be in the entire deep ultraviolet region (100–280 nm; called the UVC region). In addition, the synthesis of these high-quality semiconductors is difficult and high-cost.

Compared with other materials, gallium oxide (Ga_2O_3) is an attractive semiconductor with an inherent band gap of 4.5–4.9 eV, which is very suitable for deep ultraviolet inspection without any additional alloying processes. Among them, β-Ga_2O_3, due to its excellent chemical and thermal stability and high n-type conductivity, while meeting the requirements of good electrical conductivity and high transmittance, has shown outstanding potential in the field of photovoltaics and has been widely used in manufacturing DUV PDs. For example, Guo et al. reported that the R_λ of the β-Ga_2O_3/ZnO heterojunction photodetector is 0.35 A/W, and the EQE is 1.7×10^2% at 254 nm and 50 μW/cm^2 illumination and a bias of −5 V [14]. The metal–semiconductor–metal (MSM) β-Ga_2O_3 photodetector

with a large rejection ratio $R_{254/365\,nm}$ of $>10^6$ and a high responsivity of 29.8 A/W has also been reported by Kim et al. [15]. However, the preparation of high-quality β-Ga_2O_3 films usually requires ultra-high vacuum epitaxy techniques, including molecular beam epitaxy (MBE) [16], metal organic chemical vapor deposition (MOCVD) [17], and pulsed laser deposition (PLD) [18], which increase costs and prevent large-scale practical applications. In addition, in order to obtain high-quality thin films, lattice-matching substrates and high growth temperatures are also required. With the development of large-area photovoltaic devices, amorphous Ga_2O_3 (a-Ga_2O_3) has become more and more popular due to its low preparation process requirements, low growth temperature, no need for a lattice-matching substrate, the easy formation of large areas, and excellent photoelectric properties. Recently, the research of a-Ga_2O_3-based DUV PDs has made great progress. Xiong et al. manufactured a DUV PD with a nickel/amorphous Ga_2O_3(a-Ga_2O_3)/a-AlN/copper foil structure, which has a high response of 0.518 A/W and a response time of 0.17 seconds at a temperature of 200 °C [19]. Han et al. designed DUV PDs with an a-Ga_2O_3 phototransistor structure, which exhibited a high light-to-dark ratio of 5×10^7, a high responsivity of 5.67×10^3 A/W, and a high detectivity rate of 1.87×10^{15} Jones [18]. However, photodetectors based on a-Ga_2O_3 film still have the following problems: due to the continuous photoconductivity (PPC) effect caused by defects in the a-Ga_2O_3 film, the response speed is far from meeting the strict requirements of modern high-speed detection [20]; the device noise is very high, which severely reduces the ability to distinguish between signal and noise. Through an analysis of the previous literature, it is found that the above problems are related to the oxygen vacancies in Ga_2O_3 [21]. Oxygen vacancies in the Ga_2O_3 film are affected by the oxygen concentration, so the oxygen vacancy concentration of the Ga_2O_3 film can be reduced by adjusting the oxygen source flow rate during the growth process, but the response speed is still unsatisfactory (more than tens of milliseconds), and it is usually accompanied by a sharp decrease in responsivity [22].

In this work, by constructing an a-Ga_2O_3/p-Si heterojunction, the a-Ga_2O_3 film is treated with oxygen plasma to reduce the number of oxygen vacancies and the concentration of free carriers in the a-Ga_2O_3 film, thereby reducing the dark current and improving the photoresponsivity. Especially after the oxygen plasma treatment, the Schottky barrier between a-Ga_2O_3 and the electrode ITO can be reduced. Therefore, the photodetector can be self-powered, and its response speed is 5–10 times faster than a biased device without an oxygen plasma treatment. This work proves a simple method to improve the performance of UDV PDs and provides valuable design support for the application of thin film structure devices in the future.

2. Materials and Methods

2.1. Fabrication Process of the p-Si/Ga_2O_3 PDs

The p-type silicon wafer (1–40 Ω·cm, <100> orientation, 725 μm thickness) was firstly dipped into the diluted hydrofluoric acid solution for 3 mins to remove oxide; then, etched by KOH at 85 °C for 30 min, the etching solution consisting of KOH (2.0 wt%), isopropyl alcohol (5.0 vol%), and deionized (DI) water. Then, the obtained Si wafer with micropyramids was ultrasonically cleaned in acetone, distilled water, and ethanol for 5 min [23,24]. Finally, the cleaned substrate was blown dry in nitrogen. The chamber loaded with samples was pumped down to a base pressure of 1.4×10^{-4} Torr. Throughout the deposition process, the substrate was rotated to improve the uniformity of the film. Before depositing the Ga_2O_3 film, the silicon substrate was vacuum annealed at 650 °C for 30 min. The a-Ga_2O_3 thin film with thickness ∼305 nm was deposited on p-Si (100) using radio frequency (RF) magnetron sputtering at 100 W. An ITO film was deposited on the Ga_2O_3 film and annealed at 300 °C degrees for 8 min as the top electrode. Testing wires were connected to the electrodes by silver paste.

2.2. Oxygen Plasma Treatment

Oxygen plasma treatment was conducted before ITO growth and after Ga_2O_3 film growth. Oxygen plasma treatment technology was performed on a-Ga_2O_3 film and equipment through plasma equipment (electronic Diener plasma surface technology). The oxygen plasma treatment was performed under the parameters of a power of 60 w and an oxygen flow rate of 20 sccm, and the duration was 6 min. The controlled plasma treatment process resulted in a reduction in oxygen vacancies in the a-Ga_2O_3 film.

2.3. Material Characterization

Detailed microscopic structures of a-Ga_2O_3 film were characterized by SEM (ZEISS Ultra 55, Oberkochen, Germany) and high-resolution X-ray diffractometer (HRXRD, RIGAKU SmartLab SE, Japen 9 kW). X-ray photoelectron spectroscopy (XPS) equipped with a monochromatic Al X-ray source (97.9 W, 1486.6 eV) was used to study the chemical bonding characteristics (Thermo Fisher NEXSA, Waltham, MA, USA).

2.4. Measurements of PD Performance

Absorption spectrum of materials was measured by a UV-Vis spectrophotometer. Current–Voltage (I–V) and current–time (I–t) measurements in the dark and under UV light were performed by using a Keithley 4200 instrument. DUV light at 254 nm was provided by Luyor Lpx-254 ultraviolet lamp(Luyang, Shanghai, China), and its optical power was measured with Shanglin LS125 ultraviolet photometer.(Linshang, Shenzhen, China)

3. Results and Discussion

The device structure of the a-Ga_2O_3/p-Si heterojunction DUV PD is schematically shown in Figure 1a. It showed that the device had a roughened surface with an arrayed micropyramids structure, because the p-Si substrate was chemically etched in advance to increase the effective surface area and improve the light absorption ability of the device. The scanning electron microscope (SEM) image of a single pyramid structure is shown in Figure 1b, in which we could clearly distinguish the Si substrate and the RF-sputtered a-Ga_2O_3 film with a thickness of 305 nm. The inset of Figure 1b shows the top-view SEM image of the micro-pyramid structure. As shown in Figure 1c, the X-ray diffraction (XRD) pattern of the sample showed a strong characteristic peak which belonged to the (100) plane of the Si substrate. There was no other peaks related with Ga_2O_3. Additionally, the inset shows that, except for the broad envelope peak of about 25° from the amorphous quartz substrate, no characteristic peaks from Ga_2O_3 were observed, indicating that the sputtered Ga_2O_3 film was amorphous (a-Ga_2O_3). Figure 1d shows the absorption spectrum of the a-Ga_2O_3/p-Si heterojunction in the 190–560 nm wavelength range. The comparison with quartz glass showed that the absorption edge of the Ga_2O_3 film was located at around 250 nm, showing a strong DUV absorption and DUV light detection capabilities. The absorption edge of the samples was obtained from $(\alpha h\nu)^2$ versus $h\nu$ plots as shown in the inset in Figure 1d, where α and $h\nu$ were the absorption coefficient and photon energy, respectively. By fitting the linear region of all the plots of $(\alpha h\nu)^2$ versus $h\nu$, an optical bandgap of about 4.88 eV was derived [25].

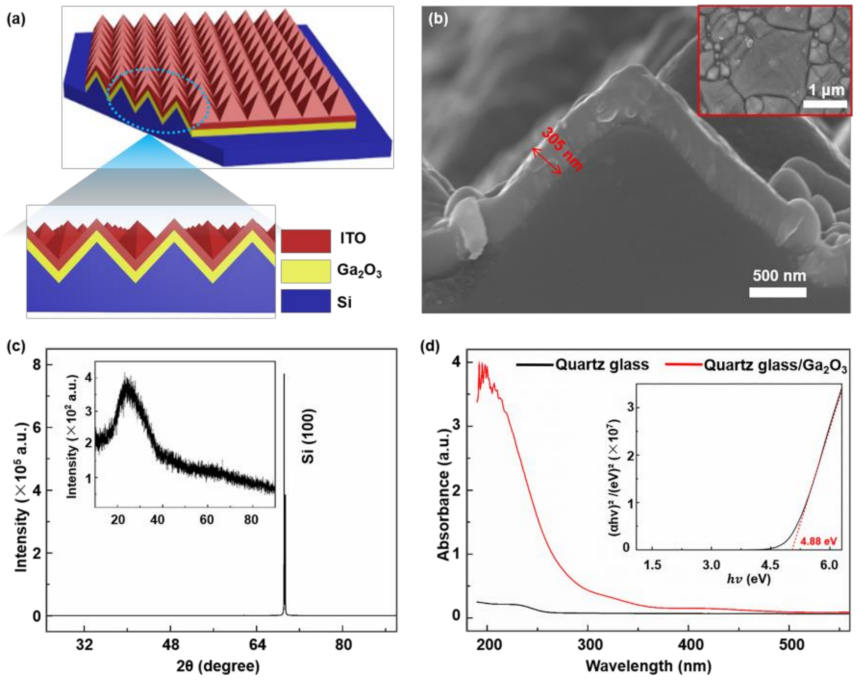

Figure 1. (**a**) Schematic diagram of the a-Ga_2O_3/p-Si heterojunctions photodetector, the enlarged view shows a cross-sectional view of the device. (**b**) SEM image of the cross-section of the Ga_2O_3 film synthesized on a pyramidal silicon substrate; upper right illustration: top view of the structure. (**c**) The XRD pattern of Ga_2O_3 film plated on Si substrate. The inset is the XRD pattern of Ga_2O_3 thin film plated on amorphous quartz substrate. (**d**) The absorption spectrum of quartz glass, quartz glass/Ga_2O_3 structure, the illustration shows the relationship between $(\alpha hv)^2$ and photon energy (hv).

Figure 2a shows the schematic diagram of the experimental setup. The optical input stimulation (254 nm UV light) was provided by a Luyor Lpx-254 ultraviolet lamp. An optical switch was utilized to provide periodical illumination upon the DUV PDs. Additionally, the effective size of the device was 3 mm × 3 mm. The bottom surface of p-Si was connected as the anode, while the ITO top layer was connected as the cathode. Figure 2b,c are the I–V curves of a-Ga_2O_3/p-Si heterojunction photodetectors under various light intensities in the range of 0–3350 mW/cm^2 for the pristine and oxygen plasma-treated device, respectively. As can be seen from the logarithmic diagram, the dark current of the detector after oxygen plasma treatment was reduced by an order of magnitude (from 1.01×10^{-3} A to 1.04×10^{-4} A). From the illustration, the device could work normally under reverse bias, and the photocurrent of both devices increased with the increase in light intensity. This could be attributed to the increased density of photogenerated carriers with the introduction of more incident photons. Photoresponsivity (R_λ) is an important parameter for describing the photoelectric performance of a photodetector, which can be described by the following Equation (1) [26,27]:

$$R = (I_\lambda - I_d)/(P_\lambda \cdot S) \quad (1)$$

where I_λ is the photocurrent, P_λ is the light power density, I_d is the dark current, and S is the effective irradiation area [28], which here was concluded to be ~0.09 cm^2. When the bias voltage was −10 V, the photoresponsivity (R_λ) and photocurrent characteristics of the detector without plasma treatment under different light intensities are shown in Figure 2d. The photocurrent increased with the increase in light intensity, and reached the maximum when the light intensity was 3350 mw/cm^2, which was 1.81 mA. The light photoresponsivity decreased with the increase in light intensity. When the light intensity was 630 mW/cm^2, the photoresponsivity was 3.7 mA/W to the maximum. Under the same

bias voltage, the photoresponsivity (R_λ) and photocurrent characteristics of the plasma-treated detector under different light intensities are shown in Figure 2e. The change trend of photocurrent and photoresponsivity was the same as that of the detector without plasma treatment. The maximum photocurrent was 1.71 mA at 3350 mW/cm^2, which was slightly smaller than that of the detector without oxygen plasma treatment. However, when the light intensity was 630 mW/cm^2, the photoresponsivity was as high as 9.97 mA/W, which was three times that of the detector without oxygen plasma treatment. This was because after oxygen plasma treatment, the oxygen vacancies in the a-Ga_2O_3 film were partially compensated [29]. The oxygen plasma treatment can provide an atmosphere with a higher oxygen concentration. The increase in oxygen content inhibited the generation of oxygen vacancies, thereby reducing the free carrier concentration. The previous literature also had similar findings [30,31]. This meant that the effective concentration of the charge carriers within a-Ga_2O_3 film was reduced, leading to a decreased dark current and an improved photoresponsivity of the heterojunction photodetector. Figure 2f shows the optical responsivity of a-Ga_2O_3/p-Si heterojunction detector in the wavelength range of 200–800 nm under a −3 V bias. This indicated that the detector exhibited a broad spectral response from the ultraviolet to the near-infrared region. Due to the sub-band gap absorption related to oxygen vacancies in a-Ga_2O_3 film, it could absorb photons smaller than its band gap (<4.88 eV), so it had photoresponse in the deep ultraviolet to near infrared region.

In order to explain the photoelectric detection mechanism of a-Ga_2O_3/p-Si heterojunction devices, the energy band of the structure was studied. Considering that the band gaps of p-Si and a-Ga_2O_3 were 1.1 eV and 4.88 eV, respectively, a band gap diagram was constructed. Under dark conditions, the oxygen plasma treatment could reduce the oxygen vacancy concentration of a-Ga_2O_3, thereby reducing the bulk resistance of the a-Ga_2O_3 film, thereby reducing the dark current of the photodetector. Under a −10 V bias, when 254 nm ultraviolet light was irradiated on the device, electron-hole pairs would be generated. The photogenerated electron–hole pair would break the equilibrium state. Light-induced holes were transferred from a-Ga_2O_3 to p-Si, and light-induced electrons were transferred from p-Si to a-Ga_2O_3, as shown in Figure 3a. Under UV light illumination, the space charge region could separate photogenerated electron-hole pairs, electrons would be transferred from Ga_2O_3 to Si, and holes would be transferred from the p-Si to Ga_2O_3 region; therefore, this photodetector could be self-powered. The technical computer-aided design (TCAD) tool Silvaco was used to simulate the photodetector in detail, including the parallel electric field-dependent model (fldmob), the Shockley–Read–Hall composite model (srh), and the Auger composite model (auger), trap composite model (trap), as shown in Figure 3b. In this procedure, due to the introduction of the Ga_2O_3/P-Si heterojunction, fldmob, a carrier mobility model that relies on parallel electric fields was introduced. When non-equilibrium carriers were added (injected) in the semiconductor due to the effect of external light, a non-equilibrium carrier recombination would occur, which would use the srh model. Auger recombination also occurred, so the Auger recombination model was used. Because Ga_2O_3 contains oxygen vacancies, trap recombination occurred, so the trap model was used. The simulated energy band was the same as Figure 3a. It could be seen from the enlarged junction area that the bending of the energy band was also the same energy band profile, which was very consistent with the above analysis.

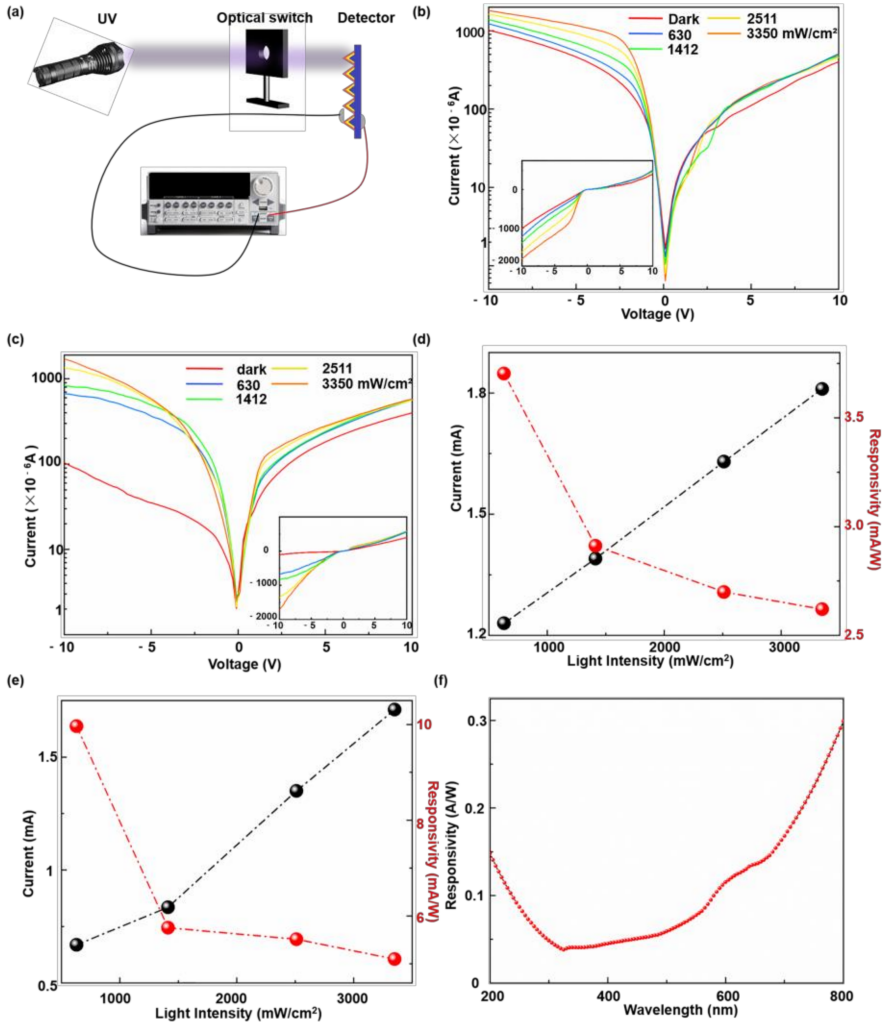

Figure 2. (**a**) Schematic illustration of the measurement configuration for photoresponse speed measurement. Under −10 V bias, the I–V characteristics of a-Ga_2O_3/p-Si heterojunction photodetectors (**b**) without plasma treatment and (**c**) after plasma treatment under dark conditions and under 254 nm illumination with different power densities in logarithmic form. The inset figure shows the I–V characteristics under the same conditions. The properties of photodetectors (**d**) without plasma treatment and (**e**) after plasma treatment under −10 V bias and 254 nm light. Left: fitting curve of the relationship between photocurrent and light intensity; right: the response of the device to various light intensities. (**f**) Under −3 V bias, the relationship between the responsivity of the plasma-treated photodetector and the wavelength.

Cycle repeatability and stability were the other two important parameters of photodetectors. In order to evaluate the stability of the photodetector, the time-dependent photocurrent of the device was measured when the ultraviolet light was repeatedly turned on and off. Figure 4 studies the photoresponse of the a-Ga_2O_3/p-Si heterojunction deep ultraviolet detector without oxygen plasma treatment and after oxygen plasma treatment to pulsed ultraviolet light. Experiments showed that the detector without oxygen plasma treatment had no response under zero bias. Figure 4a shows the transient response of a pristine detector under a −1 V bias, indicating that when the incident ultraviolet light was rapidly and repeatedly turned on and off, reversible switching between high conductance and low conductance occurred. When the frequency of the optical switch was 5 Hz, the waveform showing the reversible switching between light and dark was approximately a rectangular wave, and the rise time (τ_r, defined as the current increase from 10% of the peak value to 90%) was extracted from the single amplification cycle of Figure 4b and the decay times (τ_d, defined as the time for the current to drop from 90% of the peak value

to 10%) were 13.2 and 15.6 ms, respectively [32]. Figure 4c shows the transient response of the plasma-treated detector without applied bias. When the UV lamp was turned on, the current rapidly increased to a maximum value, followed by a fast-declining tail, and then finally stabilized. When the ultraviolet light was turned off, the current dropped sharply and then stabilized again. This waveform appeared because when the Ga_2O_3/p-Si heterojunction was irradiated with 254 nm light, photons entered the junction area, so a photoelectromotive force was formed at both ends of the p–n junction. It was equivalent to adding a forward voltage at both ends of the p junction to lower the potential barrier and generate a forward current. Therefore, the non-equilibrium state at this moment caused an upward peak current, which gradually became an equilibrium state with the length of the illumination time, which was reflected in the current stability. When the light was suddenly turned off, it became unbalanced again. At this moment, the distribution of the remaining photo-generated carriers formed an electric field that was opposite to the direction when the light was turned on, so a reverse current appeared, and then gradually stabilized [33]. The τ_r and τ_d of the device were extracted from a single amplification period of Figure 4d, which were 2.45 and 1.83 ms, respectively. The response speed of the plasma-treated detector under zero bias was 5–10 times faster than that of the non-plasma-treated detector under −1 V bias. Oxygen plasma processing caused the detector to respond at 0 V bias. It showed that oxygen plasma greatly improved the performance of the device. No obvious degradation of the device was found in the studied time scale, indicating that the photodetector had good reliability.

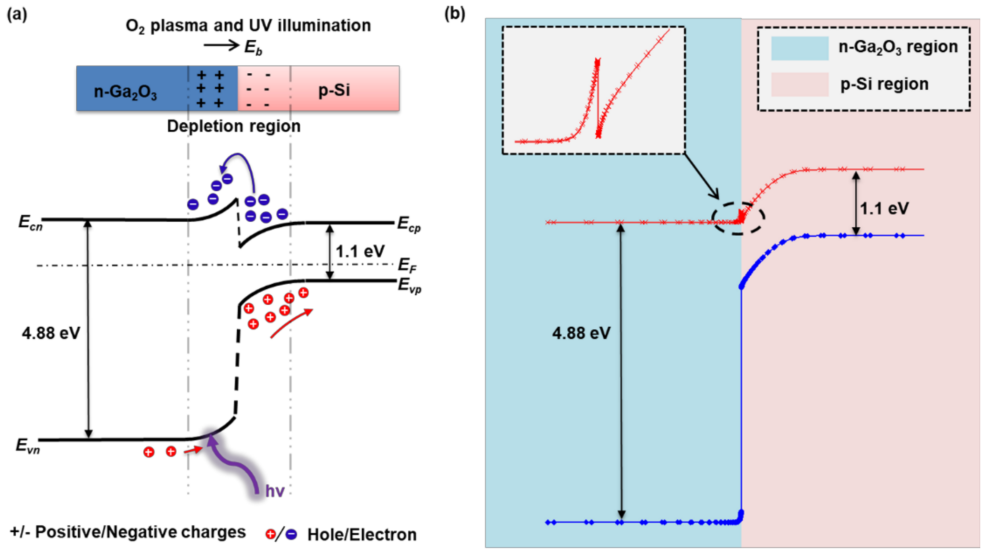

Figure 3. (**a**) The band diagram of the a-Ga_2O_3/p-Si heterojunction after oxygen plasma treatment under −10 V bias and 254 nm light source irradiation. (**b**) Using the technical computer-aided design (TCAD) tool Silvaco to simulate the energy band of the a-Ga_2O_3/p-Si heterojunction photodetector.

The reason for this optimization may be related to the number of oxygen vacancies existing in a-Ga_2O_3 film. X-ray photoelectron spectroscopy (XPS) was used to study the stoichiometry and defects of gallium oxide films. Figure 5a,b shows the oxygen 1 s nuclear XPS scanning spectra of Ga_2O_3 films in the device without oxygen plasma treatment and the device with oxygen plasma treatment, respectively. The binding energy of oxygen 1 s was approximately 531.052 and 530.795 eV, respectively [34,35]. A single oxygen 1 s peak could be deconvoluted into two different components: one was about 530.5 eV, which was related to the Ga–O bond of Ga_2O_3 [36–38], and the other was about 531.2 eV, from the lack of oxygen in the Ga_2O_3 matrix. In addition, the strength of this binding energy corresponded to the number of oxygen atoms in the stoichiometric amount of complete oxidation. Therefore, after oxygen plasma treatment, the transition to lower binding energy and the increased oxygen 1 s intensity reached the peak. This was because oxygen

plasma treatment would increase the number of Ga–O bonds and decrease the oxygen vacancy concentration.

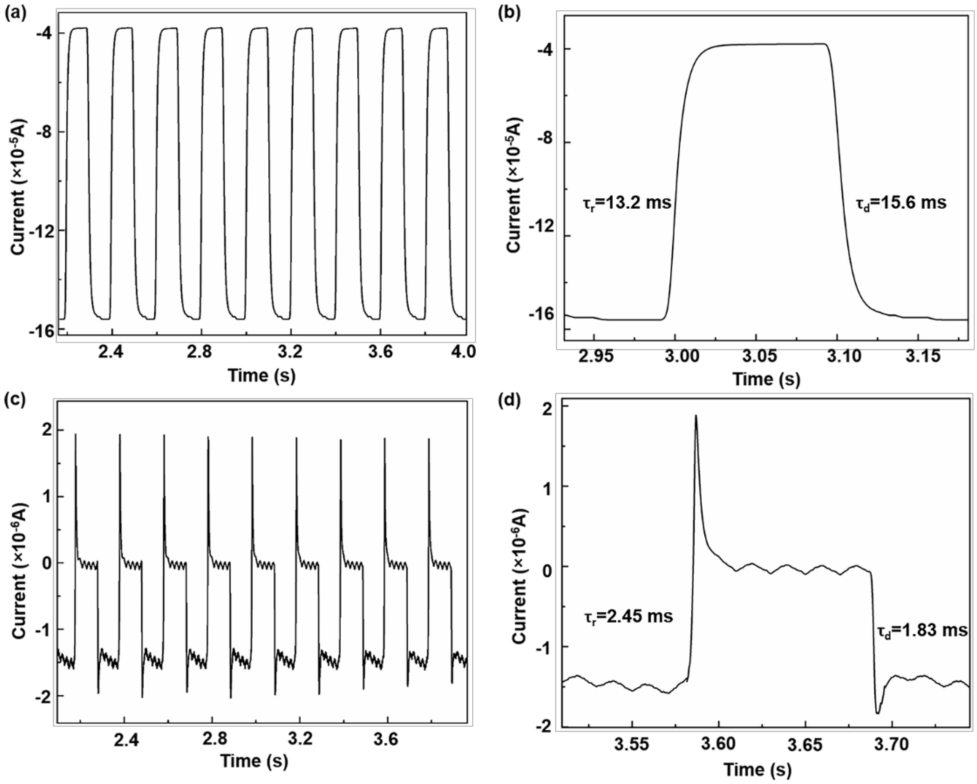

Figure 4. (**a**) The I–t characteristics of the photodetector without oxygen plasma treatment, recorded under 254 nm light, with a power density of 1.642 mW and a bias voltage of −1 V. (**b**) Amplifying a single cycle of the I–t characteristic (**a**) of the detector without oxygen plasma treatment to calculate the rise and decay time of the photodetector device excited by the 254 nm light source. (**c**) The I–t characteristics of the photodetector after oxygen plasma treatment, recorded under 254 nm light, with a power density of 1.642 mW and a bias voltage of 0 V. (**d**) Amplify a single cycle of the I–t characteristic (**c**) of the oxygen plasma-processed detector to calculate the rise and decay time of the photodetector device excited by the 254 nm light source.

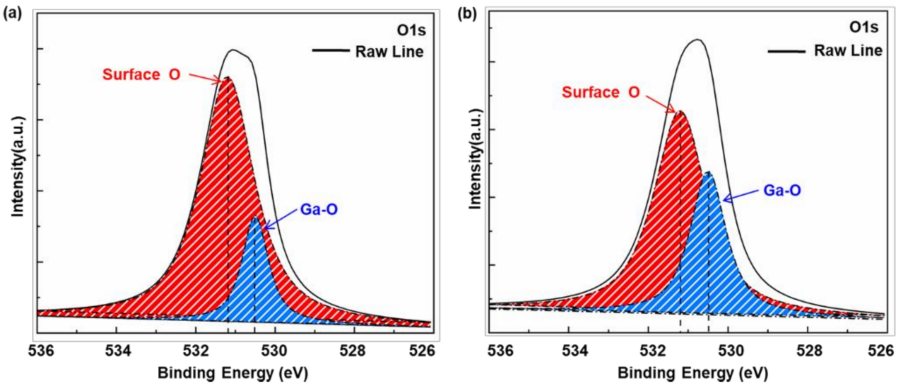

Figure 5. (**a**) High-resolution XPS spectra of O1s of Ga_2O_3 films without oxygen plasma treatment. (**b**) High-resolution XPS spectra of O1s of Ga_2O_3 film treated with oxygen plasma.

Figure 6a shows a schematic diagram of oxygen plasma treatment [39]. Figure 6b,c study the Schottky contact energy band diagram between the electrode ITO and the Ga_2O_3 thin film to illustrate the mechanism that the oxygen plasma-treated detector also

responded under zero bias. As we all know, the work function of ITO is 4.8eV, the electron affinity of Ga_2O_3 is 4.0eV, and the electrode forms a good Schottky contact on the surface of a-Ga_2O_3 [20]. A positive space charge area was formed on the surface of Ga_2O_3. The direction of the electric field was directed from the body to the surface, making the potential difference on the Ga_2O_3 surface smaller than the internal potential difference. The energy bent upwards, forming a surface barrier. Figure 6b is the energy band diagram at the electrode without plasma treatment. Since the potential barrier was too high, it could not be used as self-powered, so there was no response under 0 bias. However, under an applied voltage, electrons could pass through the Ga_2O_3 barrier and be collected by the ITO electrode.

Figure 6c is the energy band diagram at the device electrode after oxygen plasma treatment. Oxygen plasma treatment reduced the concentration of oxygen vacancies in the Ga_2O_3 film, so the number of electrons was reduced and the Fermi energy level was lowered, thereby reducing the band bending of Ga_2O_3 and the potential barrier generated by the interface. Therefore, the number of electrons that crossed the barrier and continued to flow into the ITO electrode increased, and the generated current increased.

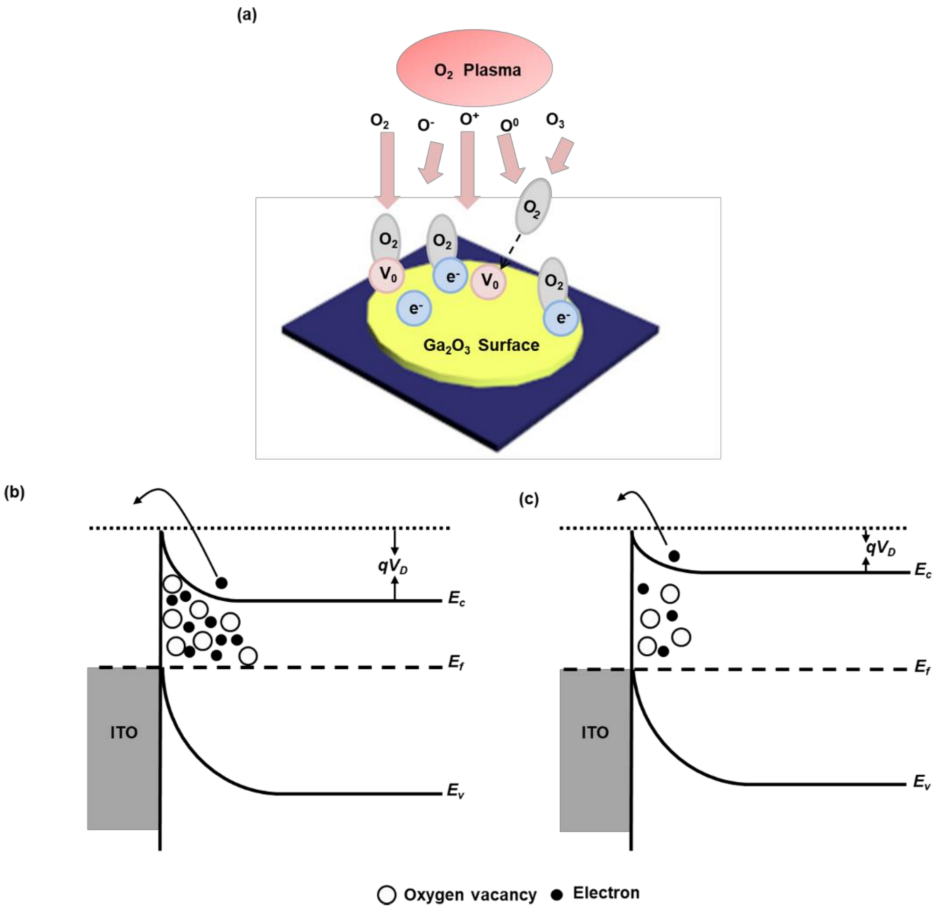

Figure 6. (**a**) Schematic diagram of oxygen plasma treatment. (**b**) The Schottky contact band diagram between the electrode ITO of the device without oxygen plasma treatment and the Ga_2O_3 film. (**c**) The Schottky contact band diagram between the electrode ITO of the oxygen plasma-treated device and the a-Ga_2O_3 film.

4. Conclusions

In summary, this paper proposed and proved a method of oxygen plasma treatment to improve the performance of a-Ga_2O_3/p-Si heterojunction DUV PDs. The main factors affecting device performance were the defect concentration of oxygen vacancies in gallium oxide and the effective Schottky barrier height between the electrode and gallium

oxide. Then, the concentration of oxygen vacancies in the a-Ga_2O_3 film was reduced by oxygen plasma treatment, so the dark current was reduced by an order of magnitude from 1.01×10^{-3} A to 1.04×10^{-4} A, and the responsivity increased from 3.7 mA/W to 9.97 mA/W. The oxygen plasma treatment also reduced the Schottky barrier between a-Ga_2O_3 and the ITO electrode, so the detector after oxygen plasma treatment also responded under 0 V bias. The response speed was that the rise time was 2.45 ms and the decay time was 1.83 ms. The unprocessed device did not respond under zero bias. Even under −1 V bias, its response speed was very slow, with a rise time of 13.2 ms and a decay time of 15.6 ms. This showed that oxygen plasma treatment was a feasible way to improve the photoresponse performance of a-Ga_2O_3/p-Si heterojunction DUV PDs.

Author Contributions: Conceptualization, X.W.; Supervision, J.D.; Validation, Y.Z.; Writing—original draft, J.C.; Writing—review & editing, L.C., M.H., X.C. and B.W. All authors have read and agreed to the published version of the manuscript.

Funding: This research was funded by National Natural Science Foundation of China 313 (11804103).

Data Availability Statement: The data presented in this study are available on request from the corresponding author.

Conflicts of Interest: The authors declare no conflict of interest.

References

1. Chen, D.; Xin, Y.; Lu, B.; Pan, X.; Huang, J.; He, H.; Ye, Z. Self-powered ultraviolet photovoltaic photodetector based on graphene/ZnO heterostructure. *Appl. Surf. Sci.* **2020**, *529*, 147087. [CrossRef]
2. Zhu, Y.; Li, J.; Ji, X.; Li, T.; Jin, M.; Ou, X.; Shen, X.; Wang, W.; Huang, F. Unintentionally doped hydrogen removal mechanism in Li doped ZnO. *AIP Adv.* **2018**, *8*, 1050147. [CrossRef]
3. Lin, C.; Lu, Y.; Tian, Y.; Gao, C.; Fan, M.; Yang, X.; Dong, L.; Shan, C. Diamond based photodetectors for solar-blind communication. *Opt. Express* **2019**, *27*, 29962–29971. [CrossRef]
4. Ouyang, W.; Teng, F.; Fang, X. High Performance BiOCl Nanosheets/TiO_2 Nanotube Arrays Heterojunction UV Photodetector: The Influences of Self-Induced Inner Electric Fields in the BiOCl Nanosheets. *Adv. Funct. Mater.* **2018**, *28*, 1707178. [CrossRef]
5. Razeghi, M.; Rogalski, A. Semiconductor ultraviolet detectors. *J. Appl. Phys.* **1996**, *79*, 7433–7473. [CrossRef]
6. Looi, H.J.; Whitfield, M.D.; Jackman, R.B. Metal–semiconductor–metal photodiodes fabricated from thin-film diamond. *Appl. Phys. Lett.* **1999**, *74*, 3332–3334. [CrossRef]
7. Nakagomi, S.; Momo, T.; Takahashi, S.; Kokubun, Y. Deep ultraviolet photodiodes based on β-Ga_2O_3/SiC heterojunction. *Appl. Phys. Lett.* **2013**, *103*. [CrossRef]
8. Xiao, X.; Liang, L.; Pei, Y.; Yu, J.; Duan, H.; Chang, T.-C.; Cao, H. Solution-processed amorphous Ga_2O_3:CdO TFT-type deep-UV photodetectors. *Appl. Phys. Lett.* **2020**, *116*, 192102. [CrossRef]
9. Tromson, D.; Bergonzo, P.; Brambilla, A.; Mer, C.; Foulon, F.; Amosov, V.N. Thermally stimulated current investigations on diamond x-ray detectors. *J. Appl. Phys.* **2000**, *87*, 3360–3364. [CrossRef]
10. Cicek, E.; McClintock, R.; Cho, C.Y.; Rahnema, B.; Razeghi, M. $Al_xGa_{1-x}N$-based back-illuminated solar-blind photodetectors with external quantum efficiency of 89%. *Appl. Phys. Lett.* **2013**, *103*, 191108. [CrossRef]
11. Chen, M.; Ma, J.; Li, P.; Xu, H.; Liu, Y. Zero-biased deep ultraviolet photodetectors based on graphene/cleaved (100) Ga_2O_3 heterojunction. *Opt. Express* **2019**, *27*, 8717–8726. [CrossRef]
12. Suzuki, R.; Nakagomi, S.; Kokubun, Y. Solar-blind photodiodes composed of a Au Schottky contact and a β-Ga_2O_3 single crystal with a high resistivity cap layer. *Appl. Phys. Lett.* **2011**, *98*, 131114. [CrossRef]
13. Li, H.; Li, P.; Zhang, H.; Chow, Y.C.; Wong, M.S.; Pinna, S.; Klamkin, J.; Speck, J.S.; Nakamura, S.; DenBaars, S.P. Electrically driven, polarized, phosphor-free white semipolar (20-21) InGaN light-emitting diodes grown on semipolar bulk GaN substrate. *Opt. Express* **2020**, *28*, 13569–13575. [CrossRef] [PubMed]
14. Guo, D.Y.; Shi, H.Z.; Qian, Y.P.; Lv, M.; Li, P.G.; Su, Y.L.; Liu, Q.; Chen, K.; Wang, S.L.; Cui, C.; et al. Fabrication of β-Ga_2O_3/ZnO heterojunction for solar-blind deep ultraviolet photodetection. *Semicond. Sci. Technol.* **2017**, *32*, 03LT01. [CrossRef]
15. Oh, S.; Kim, C.-K.; Kim, J. High Responsivity β-Ga_2O_3 Metal–Semiconductor–Metal Solar-Blind Photodetectors with Ultraviolet Transparent Graphene Electrodes. *ACS Photonics* **2017**, *5*, 1123–1128. [CrossRef]
16. Guo, D.; Wu, Z.; Li, P.; An, Y.; Liu, H.; Guo, X.; Yan, H.; Wang, G.; Sun, C.; Li, L.; et al. Fabrication of β-Ga_2O_3 thin films and solar-blind photodetectors by laser MBE technology. *Opt. Mater. Express* **2014**, *4*, 1067–1076. [CrossRef]
17. Lin, R.; Zheng, W.; Zhang, D.; Zhang, Z.; Liao, Q.; Yang, L.; Huang, F. High-Performance Graphene/beta-Ga_2O_3 Heterojunction Deep-Ultraviolet Photodetector with Hot-Electron Excited Carrier Multiplication. *ACS Appl. Mater. Interfaces* **2018**, *10*, 22419–22426. [CrossRef]
18. Han, Z.; Liang, H.; Huo, W.; Zhu, X.; Du, X.; Mei, Z. Boosted UV Photodetection Performance in Chemically Etched Amorphous Ga_2O_3 Thin-Film Transistors. *Adv. Opt. Mater.* **2020**, *8*, 8. [CrossRef]

19. Xiong, L.; Zhang, L.; Lv, Q.; Li, T.; Song, W.; Si, J.; Zhu, W.; Wang, L. Amorphous gallium oxide (a-Ga_2O_3)-based high-temperature bendable solar-blind ultraviolet photodetector. *Semicond. Sci. Technol.* **2021**, *36*, 045010. [CrossRef]
20. Cui, S.; Mei, Z.; Zhang, Y.; Liang, H.; Du, X. Room-Temperature Fabricated Amorphous Ga_2O_3 High-Response-Speed Solar-Blind Photodetector on Rigid and Flexible Substrates. *Adv. Opt. Mater.* **2017**, *5*, 1700454. [CrossRef]
21. Varley, J.B.; Weber, J.R.; Janotti, A.; Van de Walle, C.G. Oxygen vacancies and donor impurities in β-Ga_2O_3. *Appl. Phys. Lett.* **2010**, *97*, 142106. [CrossRef]
22. Zhou, C.; Liu, K.; Chen, X.; Feng, J.; Yang, J.; Zhang, Z.; Liu, L.; Xia, Y.; Shen, D. Performance improvement of amorphous Ga_2O_3 ultraviolet photodetector by annealing under oxygen atmosphere. *J. Alloy. Compd.* **2020**, *840*, 155585. [CrossRef]
23. Tanaka, H.; Takeda, M.; Sato, K. Si (100) and (110) etching properties in 5, 15, 30 and 48 wt%KOH aqueous solution containing Triton-X-100. *Microsyst. Technol.* **2017**, *23*, 5343–5350. [CrossRef]
24. Lu, H.; Zhang, H.; Jin, M.; He, T.; Zhou, G.; Shui, L. Two-Layer Microstructures Fabricated by One-Step Anisotropic Wet Etching of Si in KOH Solution. *Micromachines* **2016**, *7*, 19. [CrossRef] [PubMed]
25. Khan, N.A.; Saleem, A.; Satti, A.-U.-R.; Imran, M.; Khurram, A.A. Post deposition annealing: A route to bandgap tailoring of ZnSe thin films. *J. Mater. Sci. Mater. Electron.* **2016**, *27*, 9755–9760. [CrossRef]
26. Hatch, S.M.; Briscoe, J.; Dunn, S. A self-powered ZnO-nanorod/CuSCN UV photodetector exhibiting rapid response. *Adv. Mater.* **2013**, *25*, 867–871. [CrossRef]
27. Ding, J.; Du, S.; Zuo, Z.; Zhao, Y.; Cui, H.; Zhan, X. High Detectivity and Rapid Response in Perovskite $CsPbBr_3$ Single-Crystal Photodetector. *J. Phys. Chem. C* **2017**, *121*, 4917–4923. [CrossRef]
28. Qian, L.X.; Wang, Y.; Wu, Z.H.; Sheng, T.; Liu, X.Z. β-Ga_2O_3 solar-blind deep-ultraviolet photodetector based on annealed sapphire substrate. *Vacuum* **2017**, *140*, 106–110. [CrossRef]
29. Lany, S.; Zunger, A. Dopability, intrinsic conductivity, and nonstoichiometry of transparent conducting oxides. *Phys. Rev. Lett.* **2007**, *98*, 045501. [CrossRef]
30. Rafique, S.; Han, L.; Tadjer, M.J.; Freitas, J.A.; Mahadik, N.A.; Zhao, H. Homoepitaxial growth of β-Ga2O3 thin films by low pressure chemical vapor deposition. *Appl. Phys. Lett.* **2016**, *108*, 182105. [CrossRef]
31. Pradel, K.C.; Wu, W.; Ding, Y.; Wang, Z.L. Solution-derived ZnO homojunction nanowire films on wearable substrates for energy conversion and self-powered gesture recognition. *Nano Lett.* **2014**, *14*, 6897–6905. [CrossRef] [PubMed]
32. Liu, N.; Fang, G.; Zeng, W.; Zhou, H.; Cheng, F.; Zheng, Q.; Yuan, L.; Zou, X.; Zhao, X. Direct Growth of Lateral ZnO Nanorod UV Photodetectors with Schottky Contact by a Single-Step Hydrothermal Reaction. *ACS Appl. Mater. Interfaces* **2010**, *2*, 1973–1979. [CrossRef]
33. Chen, Y.-C.; Lu, Y.-J.; Lin, C.-N.; Tian, Y.-Z.; Gao, C.-J.; Dong, L.; Shan, C.-X. Self-powered diamond/β-Ga2O3 photodetectors for solar-blind imaging. *J. Mater. Chem. C* **2018**, *6*, 5727–5732. [CrossRef]
34. Ling, C.; Guo, T.; Shan, M.; Zhao, L.; Sui, H.; Ma, S.; Xue, Q. Oxygen vacancies enhanced photoresponsive performance of ZnO nanoparticles thin film/Si heterojunctions for ultraviolet/infrared photodetector. *J. Alloy. Compd.* **2019**, *797*, 1224–1231. [CrossRef]
35. Oanh Vu, T.K.; Lee, D.U.; Kim, E.K. The effect of oxygen partial pressure on band gap modulation of Ga2O3 grown by pulsed laser deposition. *J. Alloy. Compd.* **2019**, *806*, 874–880. [CrossRef]
36. Guo, D.Y.; Wu, Z.P.; An, Y.H.; Guo, X.C.; Chu, X.L.; Sun, C.L.; Li, L.H.; Li, P.G.; Tang, W.H. Oxygen vacancy tuned Ohmic-Schottky conversion for enhanced performance in β-Ga2O3 solar-blind ultraviolet photodetectors. *Appl. Phys. Lett.* **2014**, *105*, 023507. [CrossRef]
37. Liao, Y.; Jiao, S.; Li, S.; Wang, J.; Wang, D.; Gao, S.; Yu, Q.; Li, H. Effect of deposition pressure on the structural and optical properties of Ga2O3films obtained by thermal post-crystallization. *CrystEngComm* **2018**, *20*, 133–139. [CrossRef]
38. Peng, L.P.; Fang, L.; Yang, X.F.; Huang, Q.L.; Zhou, K.; Wu, F.; Kong, C.Y. Effect of Substrate Temperature on the Properties of Nano-ZnO: In Transparent Conductive Films. *J. Supercond. Nov. Magn.* **2010**, *23*, 881–883. [CrossRef]
39. Bazaka, K.; Baranov, O.; Cvelbar, U.; Podgornik, B.; Wang, Y.; Huang, S.; Xu, L.; Lim, J.W.M.; Levchenko, I.; Xu, S. Oxygen plasmas: A sharp chisel and handy trowel for nanofabrication. *Nanoscale* **2018**, *10*, 17494–17511. [CrossRef]